

X-RAY STUDIES OF TWO NEUTRON STARS IN 47 TUCANAE: TOWARD CONSTRAINTS ON THE EQUATION OF STATE

C. O. HEINKE, J. E. GRINDLAY, D. A. LLOYD, P. D. EDMONDS

Harvard-Smithsonian Center for Astrophysics

60 Garden Street, Cambridge, MA 02138

cheinke@cfa.harvard.edu

Draft version November 4, 2018

ABSTRACT

We report spectral and variability analysis of two quiescent low mass X-ray binaries (X5 and X7, previously detected with the ROSAT HRI) in a *Chandra* ACIS-I observation of the globular cluster 47 Tuc. X5 demonstrates sharp eclipses with an 8.666 ± 0.01 hr period, as well as dips showing an increased N_H column. The thermal spectra of X5 and X7 are well-modeled by unmagnetized hydrogen atmospheres of hot neutron stars. No hard power law component is required. A possible edge or absorption feature is identified near 0.64 keV, perhaps an OV edge from a hot wind. Spectral fits imply that X7 is significantly more massive than the canonical $1.4 M_\odot$ neutron star mass, with $M > 1.8 M_\odot$ for a radius range of 9-14 km, while X5's spectrum is consistent with a neutron star of mass $1.4 M_\odot$ for the same radius range. Alternatively, if much of the X-ray luminosity is due to continuing accretion onto the neutron star surface, the feature may be the 0.87 keV rest-frame absorption complex (O VIII & other metal lines) intrinsic to the neutron star atmosphere, and a mass of $1.4 M_\odot$ for X7 may be allowed.

Subject headings: accretion disks — binaries: close, eclipsing — binaries: X-ray — globular clusters: individual (NGC 104) — stars: neutron

1. INTRODUCTION

The primary scientific goal of neutron star (NS) mass and radius measurements are to constrain the NS equation of state (EOS) and thus internal composition (e.g., neutrons and protons vs. hyperons or free quarks). The NS EOS would be sharply constrained by a firm determination of a NS mass above $1.6 M_\odot$. This would eliminate all EOSs with significant softening (van Kerkwijk 2001). Bose-Einstein condensation of kaons, hyperons, and pions in the core would greatly soften the equation of state, leading to NSs which reach a maximum mass of $1.4\text{--}1.5 M_\odot$ (Lattimer & Prakash 2001). Mass determinations of high accuracy have been made for twelve neutron stars in binary systems using general relativistic effects, ten of them in double NS systems. Thorsett & Chakrabarty (1999) find that a Gaussian distribution with mean $= 1.35 M_\odot$ and $\sigma = 0.04 M_\odot$ well describes the masses of these NSs, with none above $1.45 M_\odot$. However, at least two NSs in accreting X-ray systems show evidence for higher masses. Vela X-1 has a reported mass of $1.86 \pm 0.32 M_\odot$ (95% confidence), though systematic deviations in radial velocity determinations continue to make this result uncertain (Barziv et al. 2001 and refs therein). Cygnus X-2 has a reported mass of $1.78 \pm 0.23 M_\odot$ (1σ), but this result depends upon the modeling of the secondary and disk light curves (Orosz and Kuulkers 1999).

Other lines of evidence also constrain NS equations of state. For instance, cooling rates of middle-aged radio pulsars imply a small range of masses around $1.4 M_\odot$ and a somewhat stiff EOS (Kaminker et al. 2001). Quasi-periodic oscillations in some low-mass X-ray binaries have sometimes been interpreted (using various models) to indicate masses near $2 M_\odot$ (see van der Klis 2000 for a review), and to force a radius less than 15.2 km (van Straaten et al. 2000). Also, calculation of the Crab pulsar's moment

of inertia (Bejger & Haensel 2002) and modeling of X-ray burst oscillations (Nath et al. 2002) suggest that only stiff EOSs are plausible. Recent attempts to fit the X-ray and optical spectrum of the isolated neutron star RX J185635-3754 seem to have ruled out all physically well-understood atmospheres, so mass and radius calculations for RX J185635-3754 remain somewhat tentative (see Burwitz et al. 2002 and references therein).

Temperature anisotropies and relatively high ($B > 10^{11} G$) surface magnetic fields are general features of model predictions for pulsar surface emission, so transiently accreting neutron stars (with much lower magnetic fields, and negligible temperature anisotropies) may provide a simpler path to determining the NS mass and radius if the thermal component can be cleanly fit. Several NSs that have been observed in outburst as soft X-ray transients have also been detected in quiescence (0.5-2.5 keV X-ray luminosity, $L_X \sim 10^{32-34}$ ergs s⁻¹), for example Cen X-4 and Aquila X-1 (van Paradijs et al. 1987, Verbunt et al. 1994). See Campana et al. (1998a) for a review of soft X-ray transients, also known as neutron star X-ray novae or quiescent low-mass X-ray binaries (qLMXBs). Spectral fits with a soft (kT=0.2-0.3 keV) blackbody (BB) spectrum, usually requiring a hard power-law tail of photon index 1-2, have been acceptable but imply an emission area of ~ 1 km radius, much smaller than appropriate for a NS surface. However, heavy elements settle out of the atmosphere on a timescale of seconds (Romani 1987), so pure hydrogen atmospheres (assuming accretion has occurred from a non-helium secondary) have been used recently to calculate the expected spectrum. Rajagopal and Romani (1996) and Zavlin et al. (1996) showed that the atmosphere of a NS shifts the peak of the emitted radiation to higher frequencies, due to the strong frequency dependence of free-free absorption. Thus a blackbody fit will derive a temperature that is too high and a radius that is

too small. Brown, Bildsten, and Rutledge (1998, BBR98; see also Campana et al. 1998a) showed that the deep crust of a neutron star transiently accreting with average rate $\langle \dot{m} \rangle$ is heated during accretion by pycnonuclear reactions, bringing the interior to a steady state temperature $\sim 10^8 \langle \dot{m} / 10^{-10} M_\odot \text{ yr}^{-1} \rangle^{0.4}$ K. This heating leads to an isotropic thermal luminosity between accretion episodes of roughly $L_q = 6 \times 10^{33} \langle \dot{m} \rangle / 10^{-10} M_\odot \text{ yr}^{-1} \text{ ergs s}^{-1}$, which BBR98 proposed as the source of the luminosity in qLMXBs (the deep crustal heating hypothesis). The power law component in qLMXBs like Cen X-4 and Aql X-1, however, has always been attributed to continued accretion (see e.g., Campana et al. 1998b).

Fits of unmagnetized ($B \lesssim 10^{10}$ G) hydrogen atmosphere models to qLMXB spectral data have been consistent with an R_∞ (R_∞ is the effective radius seen by a distant observer, $R_\infty = R/\sqrt{1 - 2GM/Rc^2}$, dependent upon M) of roughly 13 km (Rutledge et al. 1999, 2001a, 2001b). BBR98 noted that the well-determined distances to globular clusters make them ideal for determining radii of NSs in qLMXBs by this method. Recently, Rutledge et al. (2002a) have identified a promising qLMXB candidate lacking a hard power law component in ω Cen (NGC 5139). However, this object, and the soft X-ray transient in NGC 6440 (in't Zand et al. 2001), do not provide enough photons to constrain mass and radius effectively.

This picture of “deep crustal heating” as being responsible for most of the emission from quiescent neutron stars is not yet certain, however. The alternative is that accretion continues at very low levels during quiescence, either onto the neutron star surface or onto the magnetosphere, and that the energy released is directly responsible for the thermal emission (see Campana et al. 1998a). This continued accretion must not be confined to the poles to avoid producing measurable variability at the NS spin frequency, as tested by observations of Aql X-1 entering quiescence (Chandler & Rutledge 2000). Although this scenario has not yet produced detailed physical models of the spectrum and luminosity, it has received support through the observations of short-timescale variability in Aql X-1 (Rutledge et al. 2002b) and Cen X-4 (Campana et al. 1997), which cannot be explained by the “deep crustal heating” model alone. The nonthermal power-law tail spectral component also cannot be explained by deep crustal heating, and therefore suggests continued accretion. Accretion onto the neutron star surface is thought to give rise to a thermal spectrum very similar to an equilibrium hydrogen atmosphere, significantly harder than a blackbody spectrum (Zampieri et al. 1995; Deufel, Dullemond, & Spruit 2001). If accretion does indeed provide most of the X-ray luminosity in some qLMXBs, then the implied mass accretion rates ($\sim 2 \times 10^{-13} M_\odot \text{ yr}^{-1}$) may be sufficient to maintain some metals in the photosphere at levels lower than solar (Bildsten et al. 1992; Brown et al. 1998). Metals would alter the photospheric opacity, and thus the apparent radius, as well as introducing possibly observable lines into the spectrum. The lack of compelling evidence for such lines in qLMXBs (but cf. Rutledge et al. 2002b) must be considered as evidence against this scenario.

In this paper we present our spectral and temporal analysis of the two brightest ($L_X \sim 10^{33} \text{ ergs s}^{-1}$) soft sources

in the well-studied globular cluster 47 Tucanae (NGC 104). The deep ROSAT HRI survey of Verbunt & Hasinger (1998) resolved 5 sources in the central core, including X5 and X7, but had no spectral resolution. With *Chandra*'s ACIS-I instrument, we have identified 108 sources in the central $2' \times 2.5'$ region, and are able to conduct spectral analysis on a few dozen of these sources (Grindlay et al. 2001a, hereafter GHE01). We show that X5 and X7 have blackbody-like X-ray spectra, indicating that they are hot NSs. X5 has been identified with a $V = 21.6$ counterpart, which shows variability and a blue color indicative of a faint accretion disk (Edmonds et al. 2002). An upper limit for the counterpart of X7 is $V \sim 23$. Using $F_V = 10^{-0.4V-5.43} \text{ erg cm}^2 \text{ s}^{-1}$ (V band) gives F_X/F_V ratios of 46 and $\gtrsim 183$ respectively, which are typical of qLMXB systems rather than CVs. In this paper we report the detailed spectral analysis of X5 and X7, constraining the masses and radii of these NSs under the assumption of pure hydrogen atmospheres, and identifying a possible signature of low-level accretion. The large numbers of photons (4200 and 5500 from X5 and X7 respectively), well-known distance to 47 Tuc, and lack of a significant nonthermal component in their spectra allow firmer mass and radius constraints (with fewer assumptions) than previous attempts to constrain qLMXB radii.

2. ANALYSIS

The *Chandra* X-ray Observatory observed 47 Tucanae on 2000 March 16-17 for 72 ksec (in five contiguous exposures) with the ACIS-I instrument at the focus. The first, third, and last of these exposures were taken in sub-array mode to reduce the effect of pileup on bright sources (see Appendix A). We used the CIAO software package¹ to perform analysis of the point sources, as described in GHE01 and Heinke et al. 2003 (in preparation). Two of the brightest sources, identified with ROSAT as X5 and X7 (Verbunt & Hasinger 1998) are unusually soft in an X-ray color-magnitude diagram (figure 3 in GHE01) when compared with the population of (optically identified) CVs. X5 and X7 are also much brighter than the X-ray active binaries (BY Draconis and RS CVn systems) and radio-identified millisecond pulsars identified in the *Chandra* observation. X5 and X7 are each less than 1.5 optical core radii ($r_c = 23''$, Howell et al. 2000) from the center of 47 Tuc, so we consider them certain cluster members. Fits to simple blackbody (BB) spectra of X5 and X7 give implied BB radii of 1-2 km. No other sources with sufficient counts for spectral fitting in the central region of the cluster showed implied blackbody radii greater than 0.1 km.

To calculate luminosities and radii, we need estimates of the distance and N_H column. We recalculate the distance to 47 Tuc using the mean and standard deviation of the 9 recent independent distance measurements discussed in Zoccali et al. (2001, fig. 7), weighting all measurements equally. We find $(m-M)_V = 13.45 \pm .11$, $(m-M)_0 = 13.27 \pm .13$, and thus $d = 4.50 \pm .27 \text{ kpc}$ as our fiducial estimate of 47 Tuc's distance and 1σ uncertainty. The optical extinction to 47 Tuc is well-known through optical studies, which give a mean optical extinction $E(B - V) = 0.055 \pm .007$ (Gratton et al. 1997, Zoccali et al. 2001). We calculate a galactic N_H column towards 47 Tuc of $N_H = 3.0 \pm 0.4 \times 10^{20} \text{ cm}^{-2}$,

¹ Available at <http://asc.harvard.edu/ciao/>.

using $N_H/E(B-V) = 5.5 \pm 0.4 \times 10^{21} \text{ cm}^{-2}$ from Predehl & Schmitt (1995), with $R=E(B-V)/A_V=3.1 \pm 0.1$.

We find absorbed fluxes (0.5-2.5 keV) of 4.3×10^{-13} and $4.8 \times 10^{-13} \text{ ergs cm}^{-2} \text{ s}^{-1}$ for X5 (excluding eclipses and dips, see Sect. 2.1) and X7 respectively. We thus derive intrinsic luminosities for X5 and X7 of $L_X(0.5-2.5 \text{ keV})=1.4 \times 10^{33} \text{ ergs s}^{-1}$ and $1.9 \times 10^{33} \text{ ergs s}^{-1}$, and bolometric luminosities of 2.1×10^{33} and $3.4 \times 10^{33} \text{ ergs s}^{-1}$ (from the simplest hydrogen-atmosphere fits below; we note that these luminosities are model-dependent). We recalculate (assuming blackbody emission) Verbunt & Hasinger's (1998) ROSAT HRI fluxes² for X5 and X7 to be $3.5 \times 10^{-13} \text{ ergs cm}^{-2} \text{ s}^{-1}$ and $4.7 \times 10^{-13} \text{ ergs cm}^{-2} \text{ s}^{-1}$. The ROSAT-measured flux of X7 agrees well with the *Chandra* luminosity, while the ROSAT exposures of X5 probably include dips and eclipses (see sect. 2.1), which may explain the 19% smaller average flux. We conclude the observations seem to be consistent with constant luminosity over long time intervals, and thus with thermal NS emission.

2.1. Variability

The time series were analyzed using tools in the IRAF/PROS X-ray analysis package and the Lomb-Scargle periodogram (Scargle 1982). We prepared lightcurves by binning the exposure into 300 parts of 264.2 seconds each, giving an average of ~ 20 counts per bin. The lightcurve of X5 shows significant variability, in particular three clear eclipses and significant dips (Figure 1). The dips near 5 and 10 hours each show $\geq 99\%$ significance for variability, according to both K-S and Cramer-von Mises tests (Daniel 1990). The three egresses of the eclipses are sharp (less than 30 seconds, see Fig. 1a), whereas the two ingresses show a dip of roughly half the normal flux for ~ 2000 seconds before the eclipse. An epoch folding tool in PROS, `period`, gives an 8.72 hour period, but the near-total absence of flux during the eclipses (see Fig. 1) allows a simpler period calculation. We first transform the event arrival times to the solar system barycenter using the CIAO tool `xbary`. By measuring the times between two pairs of eclipse ingresses (defined as the last received photons before eclipses), and a pair of successive eclipse exits (defined as the first received photons after eclipses), we find a value of 8.666 ± 0.005 hours for the period. Measuring the eclipse lengths for the second and third eclipses as the time between the last and first received photons (excluding the sole photon halfway through the second eclipse) gives 2488 ± 12 seconds. Formal errors are the standard deviations of the measured time lengths, but are probable underestimates due to the small number of data points. The barycentered times of mid-eclipse (time system TBD) for the second and third eclipses are MJD=51619.67459 and 51620.03580.

X7 (the light curve for which is shown in GHE01) shows no significant variability, according to a K-S test. However, a period search out to a frequency corresponding to the shortest known LMXB binary period (11 minutes; 4U 1820-30, cf. Stella et al. 1987) finds a marginal peak (false alarm probability [FAP, Scargle 1982]= 5.2×10^{-2}) in the power spectrum at 5.50 hours. In the framework of the deep crustal heating hypothesis, any such period would

be most likely due to the changing N_H column, implying an intermediate inclination angle. Such a period would be believable for the type of system expected, but is of low significance. Our followup *Chandra* observations may confirm or refute it.

The lightcurve of X5 shows eclipses and dips that would not have been visible in the ROSAT data due to the lower signal-to-noise ratio (but may be visible in folded light curves; we defer this to later work). The dips directly before the eclipses suggest an accretion stream or impact point obscuring the NS, while the other dips and concomitant increases in the N_H column (see Sect. 2.2) are typical of occulting blobs in the edge of an accretion disk, as seen in dip sources (e.g., Parmar et al. 1986). Assuming a NS primary of mass $1.4 M_\odot$, and using Kepler's Third Law, the orbital separation is

$$a = 1.76 \times 10^{11} \times (0.5 + 0.5[M_2/0.3M_\odot])^{1/3} \text{ cm} \quad (1)$$

(where M_2 is the secondary mass). We can also use the length of the eclipse, the orbital separation, and the period of the system to constrain the secondary radius,

$$R \geq 3.6 \times 10^{10} \left(\frac{1.21 \times M_1}{M_1 + M_2} \right) (0.5 + 0.5(M_2/0.3M_\odot))^{1/3} \text{ cm} \quad (2)$$

Thus, for masses of $1.4 M_\odot$ and $0.3 M_\odot$ the secondary must have a radius of at least $3.6 \times 10^{10} \text{ cm}$ (using the Paczynski form of the Roche lobe radius equation, Frank, King, & Raine 1992). The size of the secondary's Roche lobe, determined by the masses and separation of the two components, must be equal to or larger than the secondary radius. This allows us to set a minimum secondary mass of $0.17 M_\odot$, for a 90 degree inclination and $1.4 M_\odot$ primary, regardless of the interior structure of the secondary. We can also geometrically constrain the inclination angle. Using $M_2 \leq 0.53 M_\odot$ from the *HST* photometry of Edmonds et al. (2002), and assuming a spherical secondary, $i \geq 76^\circ$ for a $1.4 M_\odot$ primary (or $i \geq 75^\circ$ for a $1.3 M_\odot$ primary).

The size of X5's secondary and the photometry of Edmonds et al. (2002) rules out a helium white dwarf, and indicates that the secondary is likely to be a main-sequence star. The main-sequence nature of the secondary implies the accreting material is hydrogen-rich. Rapid settling of heavy elements onto the NS surface means that for very low accretion rates (such that the observed X-ray luminosity is primarily from deep crustal heating as in BBR98) the upper layers of the atmosphere should be essentially pure hydrogen (Romani 1987). Therefore we focus on hydrogen atmosphere models for X5. The possible period of 5.5 hours for X7 also suggests a main-sequence secondary, and a hydrogen atmosphere. We note that X5's eclipsing and dipping (with increased N_H column) behavior is very similar to that of the quiescent neutron stars 4U 2129+47, as reported by Nowak et al. (2002), and MXB 1659-29 (Wijnands et al., 2002), although X5's dipping behavior seems to be less regular.

2.2. Spectra

To fit the spectra of X5 and X7 in detail, we prepared the event files without removing cosmic ray afterglows, as

² Using PIMMS at <http://asc.harvard.edu/toolkit/pimms.jsp>.

this tends to remove valid events in the cores of bright sources (*Chandra* ACIS team advice³). This change increased the total flux by <10%. We used the $\sim 2''$ regions produced by WAVDETECT to extract most ($\gtrsim 94\%$ for a ≤ 1.5 keV source) of the counts for each source, and took background spectra from nearby areas without bright sources. We excluded times in which X5 suffered eclipses and dips from our initial spectral analysis. Background and cosmic-ray contamination remains negligible, with only ~ 20 background events (estimated) compared to 4181 and 5508 total events in the X5 and X7 source extraction regions. We extracted the spectra in 205 energy bins, each 73 eV wide, giving a spectrum that is optimally oversampled by a factor of two, and grouped the spectral bins to ≥ 20 counts/bin (to ensure applicability of the χ^2 statistic) for all but the highest energy bin. Below 0.5 keV the energy calibration remains uncertain, and we have few counts (< 2%), so we fit the spectra from 0.5 to 10 keV, yielding 31 bins for both X5 and X7. The recent tool for correcting the ancillary response function for the time-dependent degradation of the ACIS low-energy QE degradation⁴ has been used in all calculations. The primary effect of correcting for this degradation is a ~ 30 -40% decrease in the required neutral hydrogen column, with the other parameters relatively unaffected. It seems unlikely that further ACIS calibration refinements will greatly affect the results we present here.

Calculations with the CIAO PIMMS software of the observed flux showed that both sources should suffer pileup: approximately 9% of X5's counts (allowing for eclipses) and 10% of X7's counts are expected to be recorded in an ACIS pixel during the 3.2 sec ACIS integration time when another photon also lands there. Pileup is a complicated problem which has not yet been thoroughly understood. We use the Davis (2001) ACIS pileup model, implemented in ISIS⁵ (Houck & DeNicola, 2000); see Appendix A for details of the pileup analysis.

We fit the spectra of X5 and X7 in XSPEC, using blackbody, Raymond-Smith, thermal bremsstrahlung, power law, and neutron star atmosphere models, each including photoelectric absorption (as a free parameter) and the Davis pileup model. We have used the unmagnetized hydrogen and helium neutron star atmosphere models of Lloyd, Hernquist, & Heyl (2002), and the unmagnetized hydrogen and solar-metallicity neutron star atmosphere models of Gänsicke, Braje, & Romani (2002)⁶ both with temperature, radius, and (gravitational) redshift as free parameters. (Redshift has not been allowed as a free parameter in previous studies of qLMXBs due to poor count statistics, but these spectra allow self-consistent constraints in redshift and radius together. See Sect. 3.2.) The atmospheric plasma (assumed to be completely ionized) affects the spectra through coherent electron scattering and free-free absorption. The models of Lloyd et al. (2002) incorporate an improved treatment of the Gaunt factors, and give similar results as the Gänsicke models within a few percent. We use both models to give an idea of the dependence of our conclusions upon model differ-

ences. We used the surface gravity (g_s) of a canonical NS, $\log g_s = 14.38$ (appropriate for a $1.4 M_\odot$, 10 km NS) although two alternative surface gravity models of D. Lloyd where $\log g_s = 14.20$ or 14.50 were also tested. The differences were found to be minor, as expected (Romani 1987, Zavlin et al. 1996), with no significant parameters affected by more than a few percent. Magnetic fields up to 10^{11} G should not affect these fits in either flux or T_{eff} (Lloyd et al. 2002). We fix the distance at 4.5 kpc; our estimated distance uncertainty (see Sect. 2) is 6%, and affects both M and R linearly. Any distance error will be the same for both sources, so for comparison we do not include distance uncertainty in Sect. 3.2 and the figures. We allow the pileup parameter α to vary freely, and note that it remains between 0.45 and 0.55, as expected from current pileup testing (see App. A).

With the pileup convolution, several single-component models (blackbody, thermal bremsstrahlung, power law, and the NS atmosphere models, all with photoelectric absorption as a free parameter) fit the spectra of X5 and X7 reasonably well (null hypothesis prob. > 5%). No Raymond-Smith thermal plasma model with abundances above 1% solar fit the data acceptably. Single-component power-law models require a spectral photon index > 5 , which would be highly unusual (pulsars with power-law X-ray spectra generally display indices ~ 1 -3). Thermal bremsstrahlung models require kT below 600 eV, which is much softer than in cataclysmic variables (CVs) that display high X-ray luminosity (Eracleous et al. 1991), and the F_X/F_V ratios are higher than those of known CVs. Although we cannot formally exclude the blackbody models, we note difficulties with this model: the derived radii are rather small (while the lack of X-ray pulsations in other qLMXBs suggests that the emission is isotropic, Chandler & Rutledge 2000), and recent accretion is expected to leave an atmosphere of H or He on the NS. We include parameters for blackbody fits in Table 1 for comparison with previous studies. Helium atmospheres are ruled out for X5 due to the main sequence nature of the companion (Edmonds et al. 2001). We note that tests of D. Lloyd's He atmosphere models forced much higher redshifts for standard radii than obtained below for both neutron stars, leading to inconsistency with the causality constraint. The hydrogen atmosphere models give temperatures of order 10^6 K, and the best fits imply masses and radii in the range expected of neutron stars, leading to our focus upon these models. Using solar metallicity photoelectric absorption, the fits for X5 give $\chi^2_\nu = 1.38$ with 26 degrees of freedom (dof), for a null hypothesis probability (prob)=10%. For X7, we obtain $\chi^2_\nu = 1.20$, 26 dof, prob=22%. The spectra of X5 and X7 along with the Lloyd H-atmosphere model predictions and the fit residuals are plotted in Figure 2.

The photoelectric absorption ($N_H = 3.0 \pm 0.4 \times 10^{20} \text{ cm}^{-2}$) derived from optical studies (see Section 2) is ruled out for both sources at 90% confidence. For X7, $N_{H,22} > 0.09$ ($N_{H,22} = N_H/10^{22} \text{ cm}^{-2}$) is required, while $N_{H,22} > 0.04$ for X5. We fit separately the intervals of X5's spectrum which showed dips (count rate < 13 cts

³ Available at <http://www.astro.psu.edu/xray/acis/recipes/>

⁴ See http://cxc.harvard.edu/cal/Acis/Cal_prods/qeDeg/.

⁵ ISIS is available at <http://space.mit.edu/CXC/ISIS/>.

⁶ Available at <http://heasarc.gsfc.nasa.gov/docs/xanadu/xspec/models/gbr.html>

bin⁻¹, see Fig. 1), and those which did not. The dipping portions (with 19% of the total counts) showed $N_{H,22}$, $0.24^{+0.08}_{-0.14}$ (compared to $N_{H,22} = 0.09 \pm 0.05$ outside dips) when T_{eff} and z are held equal to the best values outside dips. We use the times outside dips for all other fits in this paper.

We applied the best-fitting hydrogen atmosphere spectral fits from the full datasets to the subarray exposures of X7 and X5. Freezing all parameters except the pileup parameter α , we obtained $\chi^2_{\nu}/\text{dof}=1.36/11$, prob=18% for X5, and $\chi^2_{\nu}/\text{dof}=0.76/11$, prob=68% for X7. These fits to the full datasets are shown with the subarray data in Fig. 3. The agreement between the subarray and full dataset parameters demonstrates that the pileup formalism is valid. We use the complete datasets (minus X5's eclipses and dips) for the remainder of this paper, as the subarray fits are poorly constrained due to the lack of counts.

2.3. Possible Edges and Power-Law Constraints

We then performed spectral fits adding photoelectric absorption of gas with the nominal metallicity of 47 Tuc (20% solar for iron-group, 40% solar for α -group elements, taken to be calcium and below, Zoccali et al. 2001) to the known galactic absorption column. However, the fits become poorer for X7 as metallicity in the excess gas decreases, due to a negative residual near 0.7 keV. X5 produces $\chi^2_{\nu}/\text{dof}=1.21/31$, null hypothesis probability (prob.) of 8%, and X7 produces $\chi^2_{\nu}/\text{dof}=1.41/26$, prob. 11%. Adding an absorption edge improves the residuals for both X5 and X7 (see Fig. 4), and increases the null hypothesis prob. values to 18% and 83%. The edge energy is best fit at 660^{+45}_{-67} eV for X5 and 632^{+36}_{-52} eV for X7 (90% conf. intervals). The F-test calculator in XSPEC gives 9.7% and 0.02% as the respective probabilities that X5 and X7 do not require the additional component (but see Protassov et al. 2002 for limitations of this statistic). This makes the feature in X5 marginal at best, but the similarity to X7 is very suggestive. The solar metallicity photoelectric absorption fits are similarly improved by the addition of the edge. Other sources in 47 Tuc (CVs with more complex spectra; Heinke et al. 2003 in prep) do not seem to show a similar edge, arguing against an instrumental interpretation. Nevertheless, we also continue to consider the simpler hydrogen atmosphere with solar metallicity absorption model, for comparison with results from other systems. We show results for spectra using 47 Tuc metallicity gas and an edge with parameters free in Table 1, along with results using solar metallicity gas, and a black-body with 47 Tuc metallicity gas and edge.

Subtracting a gaussian (modeling an absorption line) instead of fitting an edge also improves the fits to $\chi^2_{\nu}=0.98$ for X5, and $\chi^2_{\nu}=0.75$ for X7. The gaussian line energies are best fit at $0.74^{+0.03}_{-0.03}$ keV and $0.71^{+0.03}_{-0.04}$ keV for X5 and X7 respectively, with $\sigma < 90$ eV for both. This gives a better fit to X5 than the edge model. However, since hydrogen-atmosphere incandescent neutron stars should not have cyclotron lines (as their fields should be too low), nor any atomic transition lines (such as discussed in Sanwal et al. 2002), the subtraction of gaussians is not physically motivated for a pure hydrogen atmosphere in the deep crustal heating model. If the features are indeed atomic lines,

then the atmosphere is not pure hydrogen and the models will not accurately describe the NS radii, as discussed in Section 3.2. We discuss the possibilities for the edge in Section 3.1.

The qLMXBs Cen X-4 and Aql X-1 have generally shown a hard power-law tail, of photon index 1-2, which predominates over the thermal component above 2 keV. Such a tail is absent from X5 and X7, where the energy received above 2 keV can be attributed wholly to pileup. The subarray exposures show only 3 or 4 counts (out of 369 or 423 counts for X5 and X7 respectively) beyond 2.5 keV. An F-test of the confidence for addition of a hard power-law component with photon index of 1.5 gives $F=1.56$ for X5 and $F=0.2$ for X7, indicating the component is not required (probability of achieving these F-values by chance if the component is not real is 22 and 66% respectively). In Figure 5, the best hydrogen-atmosphere fits to X5 and X7 with an added PL of index 1.5 are shown, in an XSPEC νF_{ν} plot for ease of comparison with other results. The upper limit to power law component flux in the 0.5-10 keV band is only 0.6% of the total flux for X7, and 4% for X5.

3. DISCUSSION

3.1. Edge possibilities

The possible edge identified in the spectra of X5 and X7, if unredshifted, is most likely identified primarily with the OV edge, at 0.627 keV. This edge would suggest gas at temperature $T \sim 3 \times 10^4$ K (Kallman & McCray 1982), which we speculate may be a wind from the disks. Assuming a wind of density structure $\rho = \rho_0 R^{-2}$, the ionization parameter of the wind $\xi = L/nR^2$ remains constant until the wind is slowed by interactions with the cluster medium as the wind's density approaches the cluster gas density ($n_e = 0.067 \text{ cm}^{-3}$, Freire et al. 2001) at $R_{out} \sim 10^{16}$ cm. The mass loss rate in the wind outflow can then be calculated, using

$$\dot{M} = \frac{M_{tot}}{\delta t_{Rin-Rout}} = \frac{4\pi\rho_0 R_{out}}{R_{out}/v} \quad (3)$$

where M_{tot} is the total gas mass in the correct ionization state (considered to be the wind density structure out to R_{out}), and v is the gas velocity.

Using 40% solar abundance for oxygen in 47 Tuc (Zoccali et al. 2001), and a K-shell photoionization cross-section for OV of $\sigma=0.47 \times 10^{-18} \text{ cm}^2$ (Daltabuit & Cox 1972), we find that the optical depth $\tau = \kappa \int \rho(R) dR = 40\rho_0 R_{in}^{-1}$. If we choose $R_{in} = 10^{10}$ cm (which is 1/4 of the circularization radius of the disk) and optical depths from Table 1, we derive $\xi \sim 10$, which is sufficient to keep O in the OV state. A wind extending from $R = 10^{10}$ out to 3×10^{16} cm reproduces the edges' optical depth, giving a total ionized wind mass of $\sim 10^{-9} M_{\odot}$ for both systems. We can also derive

$$\dot{M} = 8.1 \times 10^5 \tau R_{in} \text{ g s}^{-1} = 1.3 \times 10^{-20} \tau R_{in} M_{\odot} \text{ yr}^{-1} \quad (4)$$

by mass conservation (from eq. 3) and using the gas sound speed $v = \sqrt{3kT/m_p} = 2.7 \times 10^6 \text{ cm s}^{-1}$. This leads to a mass loss rate of order $5 \times 10^{-11} M_{\odot}/\text{yr}$. This is significantly more than the highest allowed (by its quiescent luminosity) current low-level accretion rate of the neutron

star ($2 \times 10^{-13} M_{\odot} \text{ yr}^{-1}$). This suggests that most of the material in the accretion disk is swept out by winds instead of ever reaching the neutron star (see Sect. 3.3). We note that this mass loss rate is of the same order as the time-averaged accretion rate necessary to heat the neutron stars to an incandescent luminosity of a few $10^{33} \text{ ergs s}^{-1}$ (BBR98; see Introduction).

This calculation demonstrates the plausibility of this model, but of course other scenarios cannot be ruled out. Another obvious possibility is that the edge represents the prominent 0.9 keV OVIII photoionization edge (blended with other metal lines; BBR98) in neutron star atmospheres with nonzero metallicity, gravitationally redshifted by a factor $(1+z)$ of 1.35 to 1.43 (reasonable for canonical NSs). This inspired us to attempt to fit a solar-metallicity neutron star atmosphere model, produced by Gänsicke, Braje, & Romani (2002), with absorbing N_H columns for either solar-metallicity or 47 Tuc-metallicity absorption. These models were not successful, generating $\chi^2_{\nu} = 1.3$ with 32 dof for X5 (requiring $N_H > 2 \times 10^{21}$) and $\chi^2_{\nu} = 2.3$ with 29 dof for X7. However, subsolar metallicity neutron star atmospheres (implied by the known metallicity of 47 Tuc) have not yet been calculated, and may fit these data.

3.2. Constraints on mass and radius

The “radiation radius” R_{∞} , as seen by an observer at distance D , is calculated by measuring the observed flux and temperature. Using $F_{\infty} = \sigma(R_{\infty}/D)^2 T_{\infty}^4$ and $T_{eff} = T_{\infty}(1+z)$ (e.g., Lattimer & Prakash 2001), where z , the gravitational redshift of a star with mass M and true radius R , is given by $z = -1 + 1/\sqrt{1 - 2GM/Rc^2}$, we get

$$R_{\infty} = \frac{D \times (1+z)^2}{T_{eff}^2} \sqrt{\frac{F_{\infty}}{\sigma}} \quad (5)$$

The true radius R is recovered with $R = R_{\infty}/(1+z)$. The normalization of the Lloyd models is conveniently expressed as $\text{norm} = (R [\text{km}]/D[10 \text{ kpc}])^2$, while that of the Gänsicke models is expressed as $d[\text{pc}]/R[10 \text{ km}] = 1/\sqrt{\text{norm}}$, or $R[\text{km}] = 10 d[\text{pc}] \sqrt{\text{norm}}$. Thus the true radius can be straightforwardly calculated from the normalization parameter alone. The mass can then be derived using $M = Rc^2(1 - (1+z)^{-2})/(2G)$.

The surface gravity $g_s = GM(1+z)/R^2$ is used to calculate the opacity of the hydrogen atmosphere. The sense of alterations in the surface gravity is that a lower surface gravity model gives a slightly cooler temperature, and thus requires a lower redshift to fit the data than a higher surface gravity model. This is a relatively small effect due to increased pressure ionization with gravity (Romani 1987), and alters mass and radius estimates by less than 10% in the region of parameter space of interest. In this section we use models with $\log(g_s)=14.38$, appropriate for a $1.4 M_{\odot}$, 10 km NS.

The X-ray color magnitude diagram for 47 Tuc (Figure 2 in GHE01) shows that while X7 is brighter than X5, it is also significantly softer. This effect cannot be attributed solely to a hard PL component in X5, nor to pileup (pileup hardens the raw spectrum, and the brighter X7 has slightly more pileup), nor to differences in N_H column. The spectral difference is confirmed by the significant difference in the best-fit blackbody temperature between X5 and X7

(see Table 1). If one holds z constant at 0.306 (appropriate for $M=1.4M_{\odot}$ and $R=10 \text{ km}$), the lower temperature for X7 would require a significantly larger radius. However, an effect of increasing the gravitational redshift is to lower the apparent temperature of the NS surface, and thus to bring the two spectral fits to similar radii. The assumption of the relation $z=0.306$ does not encompass the full range of neutron star EOS predictions even if $M=1.4M_{\odot}$. Thus we allow redshift to vary in our fitting procedure, and explore the space in M and R that is allowed by the constraints on z and normalization.

The 90% confidence contours in M - R space are plotted for X5 (red dotted) and X7 (blue dashed) using simple solar-metallicity photoelectric absorption and the Lloyd et al. (2002) hydrogen-atmosphere model, in figure 6a. The same contours are shown in figure 6b for the Gänsicke hydrogen atmosphere model. In figure 7, the contours for X5 and X7 are shown using absorbing gas set to 47 Tuc metallicity, with an absorption edge (7a uses the Lloyd model, 7b uses the Gänsicke model). A sample EOS, the APR model (Akmal et al. 1998) is also plotted, as is the causality constraint (above which the required sound speed exceeds the speed of light). The M - R space above the causality line cannot contain NSs under any EOS.

X5 is well-fit by a $1.4 M_{\odot}$ 10 km NS, while X7 is not consistent with masses below $1.8 M_{\odot}$ for typical NS predicted radii between 9 and 14 km, using either the solar metallicity absorption fits or 47 Tuc metallicity absorption fits with an edge. Some spectral fits (fig. 7a) require X7 to have a mass exceeding $3 M_{\odot}$ at 90% confidence. For a standard radius of 10 km, we have calculated the 90% mass range for both X5 and X7 in Table 1. We have also calculated the radius range for an assumed redshift of 0.306; the large radii required for X7 exclude the possibility of a strongly heated polar cap. We note that the models of Gänsicke et al. (2002) slightly decrease the large mass or radius of X7, since they give slightly higher temperatures. The difference between the Gänsicke and Lloyd models is small, but leads to significant differences in the mass and radius ranges. We give the 90% mass and radius ranges as above for the Gänsicke models also (see Table 1) as an indication of the range in models, and plot the 90% contours derived from both the Lloyd and Gänsicke models in figures 6 and 7. Lloyd model fits to X7 with 47 Tuc metallicity gas and no edge (less likely due to the poorer quality of these fits, see Sect. 2.2) also require a mass of $2.32^{+0.15}_{-0.19} M_{\odot}$ for a 10 km radius. Similar Gänsicke model fits allow a mass of $2.11^{+0.16}_{-0.45} M_{\odot}$. Lloyd model fits with a gaussian absorption line require a mass of $2.29^{+0.14}_{-0.05} M_{\odot}$, while equivalent Gänsicke model fits require a mass of $2.18^{+0.14}_{-0.02} M_{\odot}$ for the same 10 km radius assumption. *Thus none of our spectral fits allow for X7 to have the canonical NS mass and radius.*

The implication that X7 is more massive than the canonical NS range (1.3-1.45, Thorsett & Chakrabarty 1999) is very interesting. Two possibilities for the increased mass present themselves. X7 may have been born more massive than most NSs (see e.g. Timmes, Woosley & Weaver 1996), or it may have accreted significant mass from its companions over its long life. Observations of either type of massive NS are more probable in globular clusters compared to the field. Initially massive NSs ($> 1.8 M_{\odot}$) can-

not find their way into relativistic NS-NS binaries (which have the best mass determinations) because such systems require a common-envelope stage, and massive neutron stars probably descend from stars over $20 M_{\odot}$ which do not pass through a red giant stage (see Barziv et al. 2001). Alternatively, a NS in a dense globular cluster has many chances to accrete mass from its numerous companions over its long life (see Hurley & Shara 2002, Grindlay et al. 2002), possibly leading to massive NSs as inferred in some LMXBs (e.g. Orosz and Kuulkers 1999). The objection that observed MSPs, probable descendants of LMXBs, are not more massive than $1.4 M_{\odot}$ (Thorsett & Chakrabarty 1999) can be answered if accretion of substantial ($> 0.1 M_{\odot}$) mass buries the magnetic field of the NS. In either case, confirmation of a NS more massive than $1.8 M_{\odot}$ would immediately exclude many NS equations of state (see Lattimer & Prakash, 2001).

However, we note a possible problem with the possibility that X7 is more massive than $1.8 M_{\odot}$. Its continued brightness over thirty years in which it was not observed to be actively accreting suggests that it does not experience enhanced URCA cooling, while some other NSs may require direct URCA cooling to explain their low luminosity (Cen X-4, Colpi et al. 2001; SAX J1808.4-3658, Campana et al. 2002). More massive neutron stars are expected to cool faster due to the higher density in their cores (see Kaminker et al. 2001), so one would expect X7 to be dimmer than most qLMXBs if its accretion history is similar. Of course, X7 could spend a larger fraction of its history accreting at high rates, explaining the apparently high core temperature. Or most LMXBs could be as massive as X7 (as implied by some QPO results, van der Klis 2000).

Alternatively, both X7's apparently high mass and/or radius and the ~ 0.64 keV possible absorption features in both X5 and X7 may be explained if X5 and X7 derive a substantial portion of their X-ray luminosity from continued low-level accretion. Accretion at rates sufficient to produce $L_X \sim 10^{33}$ ergs s $^{-1}$ would also be sufficient to maintain metals in the photosphere, altering the opacities slightly closer to a blackbody and leaving a pronounced O VIII edge (combined with other metal edges) at $0.87/(1+z)$ keV. Although solar-metallicity NS atmospheres do not fit the data well, subsolar-metallicity NS atmospheres (not yet calculated) may. Such models would predict smaller radii and/or masses for X7 than our hydrogen-atmosphere fits, perhaps consistent with canonical NS predictions. These models would need to self-consistently calculate the effects of accretion at low rates on the emerging NS spectrum, and would suffer from uncertainties in the metallicity of accreting matter.

3.3. Power law and accretion

One of the major results of this study is the result that the quiescent LMXBs X5 and X7 show very little or no hard power-law spectral component, unlike most field qLMXBs. A lack of evidence for a PL tail has also been noted in the qLMXBs CXOU 132619.7-472910.8 in ω Cen (Rutledge et al. 2002a) and U24 in NGC 6397 (Grindlay et al. 2001b), but X5 and X7 allow much tighter limits on the PL component. Although the origin of the PL component is unclear, no explanation from deep crustal heating has

been given, so it is generally assumed to be due to continued ADAF-like low-level accretion (e.g., Campana 1998a, Rutledge et al. 2001b, 2002a). We note that the spectra and luminosities of black hole accretion disks in quiescence are similar to the PL component alone in qLMXBs containing NSs (power laws with spectral index $\alpha \sim 1-2$ and $L_X \sim 10^{30-33}$; Kong et al. 2002), perhaps implying a similar accretion-related origin for both. Within the deep crustal heating explanation for the thermal emission, the lack of a power law component and lack of variability in X5 and X7 suggest that accretion onto the NS surface is held at a very low level or completely stopped. Low binary mass transfer rates compared to Cen X-4 and Aql X-1 could explain the relatively weak power law and lack of outbursts in X5 and X7. However, if the deep crustal heating model is correct, the current X-ray luminosity will depend upon the long-term ($\lesssim 10^{4-5}$ years) accretion history of the NS. The low mass transfer explanation fails to account for the higher luminosity of X5 and X7, $L_X(0.5 - 10\text{keV}) \sim 10^{33.2}$, compared to $\geq 10^{32.2}$ for the more active Cen X-4 (Rutledge et al. 2001a). And accretion to the disk is clearly continuing in X5, as shown by the dips and blue optical color of the companion (Edmonds et al. 2002).

It is possible that little to no mass from the disk is reaching the neutron star, but is instead being driven from the system in a wind, as in the ADIOS solutions for black hole accretion (e.g., Blandford & Begelman 1999, and see Menou & McClintock 2001). The relative lack of accretion onto the neutron star surface could be explained by a propeller effect (when the magnetospheric radius expands beyond the corotation radius and expels inflowing material; Illarionov & Sunyaev 1975) or a pulsar wind. The shock generated by a propeller effect, or the shock from a pulsar wind at lower accretion rates, could also provide an explanation for the hard power law X-ray emission (see Campana & Stella 2000). The transition to a propeller effect in the expected luminosity range ($L_X \sim 10^{36}$ ergs s $^{-1}$) may have been observed in Aql X-1 (Zhang et al. 1998, Campana et al. 1998b; but cf. Maccarone & Coppi 2002, and Chandler & Rutledge 2000) and 4U 0115+63 (Campana et al. 2001). A pulsar wind is thought to eject matter falling from the Roche-lobe overflowing secondary in the millisecond pulsar PSR J1740-5340 in NGC 6397 (Burderi et al. 2002). The advent of a pulsar wind may sweep away the entire accretion disk due to the radial dependencies of the pulsar radiation pressure and the disk pressure (Burderi et al. 2002). However, this assumes a standard Shakura-Sunyaev disk structure throughout the entire disk. Due to dynamical encounters in globular clusters (cf. Grindlay et al. 2002), it may be possible to cycle between pulsar emission and accretion regimes.

We note a possible correlation between the existence of a strong power law component and recent (suggesting frequent?) outbursts. Cen X-4, Aql X-1, CX1 in NGC 6440 (in't Zand et al. 2001), KS 1731-260 (Wijnands et al. 2001), and 4U 2129+47 (Nowak et al. 2002) each have strong PL components and recorded (recent) outbursts, while X5 and X7, U24 in NGC 6397 (Grindlay et al. 2001b), and CXOU 132619.7-472910.8 in ω Cen (Rutledge et al. 2002a) have exhibited evidence of neither (although the limits on the 6397 and ω Cen sources' PL components

are currently weak). This may indicate a difference in the mode or level of accretion activity between the two groups.

4. CONCLUSIONS

The X-ray sources X5 and X7 are thermally radiating neutron stars with hydrogen atmospheres, probably heated by transient accretion. X5 shows eclipses, which allow parameters of the binary system to be inferred. Both X5 and X7 are well-fit by the hydrogen atmosphere model spectra of Gänsicke et al. (2002) and Lloyd et al. (2002), absorbed by a column of gas with the known cluster metallicity and displaying a possible absorption feature near 0.64 keV tentatively identified with an OV edge. The feature may instead be intrinsic to the neutron star atmosphere, in which case it is most likely identified with the 0.87 keV (rest-frame) complex of oxygen and metal lines in a subsolar-metallicity neutron star atmosphere. A hard power-law component to the spectra, such as has been observed in other qLMXBs, is extremely weak or non-existent in X5 and X7. The well-known distance to 47 Tucanae allows modeling of the neutron star atmospheres to constrain a space in mass and radius for each, if the atmospheres are purely hydrogen. Fits using the ISIS pileup model and hydrogen atmosphere fits require X7 to be more massive than $1.8 M_{\odot}$ for the range of radii 9-16 km, while the constraints on X5 are consistent with a mass of $1.4 M_{\odot}$ for a wide range of radii. However, if the majority of the X-ray luminosity is derived from low-level accretion, then appreciable amounts of metals would remain in the neutron star atmospheres. In addition to producing the feature near 0.64 keV, the metals would alter the overall

shape of the spectrum slightly closer to a blackbody, possibly allowing both X5 and X7 to fit a canonical NS mass and radius. If accretion is not continuing, a high mass for X7 is unavoidable.

A series of observations (~ 300 ksec total) in October 2002 with *Chandra*, using the back-illuminated ACIS-S chips for greater sensitivity below 4 keV, will give us more data with which to constrain the mass and radius, and mode of emission, of these neutron stars. We will be particularly interested in looking for intrinsic variability, and confirming or refuting the possible edge feature. The eclipsing behavior of X5 also allows the possibility of using *HST* to measure the radial velocity of the secondary, constraining the mass of X5. Unfortunately optical spectroscopy of X7 is beyond the reach of *HST*, due to crowding (Edmonds et al. 2002). These demonstrations of fits with hydrogen atmosphere models show that the project of constraining the neutron star equation of state through spectral fitting holds particular interest for these two systems.

This work was supported in part by *Chandra* grants GO0-1098A and GO2-3059A. C.H. thanks M. Nowak, J. E. McClintock, J. Raymond, J. McDowell, F. Walter, P. Konradt, and J. Lattimer for helpful discussions. C.H. also thanks M. C. Miller for EOS relations, the anonymous referee for helpful suggestions, B. Gänsicke and K. Arnaud for assistance with XSPEC implementation of NS models, and especially J. Houck for assistance with ISIS. We thank the *Chandra* ACIS team at Penn State and the CXC team at the CfA for advice on data analysis.

APPENDIX

TREATMENT OF PILEUP EFFECTS

Since X5 and X7 possess soft spectra, cut off below 1 keV by the falling detector response and neutral hydrogen absorption, their raw spectra can be modeled to zeroth order as gaussians with peaks at energy ~ 1 keV and widths of $\sigma \sim 0.3$ keV from a simple fit to the pulse height data. Thus, the pileup will produce a secondary peak at ~ 2 keV with $\sigma \sim 0.4$ keV, containing 9% and 10% for X5 and X7 respectively of the total received flux, neglecting grade migration. (Grade migration occurs when the charge clouds from two photons are recorded at the same time in adjacent pixels, and the pattern of charge is assigned an inferior grade, leading to the discarding of the event; see Davis 2001). This secondary peak was misinterpreted in GHE01 (where pileup was ignored) as a high energy tail. We added a gaussian component to model the pileup component of the spectra, allowed the parameters to vary freely, and discovered that the best-fitting gaussian component gave a median energy of 2.23 or 2.25 keV for X5 and X7, $\sigma=0.38$ keV for both, and a total flux fraction (considering that the effective area at 1.1 and 2.2 keV differs by a factor of 3/5) of 9% and 10%, respectively. The addition of this gaussian improved the reduced chi-squared statistic by a factor of 2-4 for any single or multiple-component spectral model we tried, and the close agreement of the empirical parameters with the expected ones confirms this simple pileup model. We note that such a simple model is only fortuitously valid for X5 and X7 since they lack significant hard spectral components, as discussed in Sect. 2.3.

A more complete treatment of pileup is offered in the Davis (2001) model of ACIS pileup⁷. This has been implemented separately in XSPEC (Arnaud et al. 1996) v. 11.1, and the MIT spectral analysis system ISIS. Comparison of the two systems suggested that, at the time of our analysis, the ISIS implementation produced more accurate values for the source model parameters⁸, so we used the ISIS system for our spectral analysis. The Davis pileup model parametrizes grade migration by assuming that the good grade fraction of piled-up events is proportional to $\alpha^{(p-1)}$, where p is the number of photons in one event detection cell during one frame time. We used a piled psf fraction (psfrac) of 0.95, and fixed g_0 (the good grade branching parameter) at 1.0 following Davis (2001), while the parameter α was allowed to vary. In effect this alters the normalization of the pileup bump for this low-pileup exposure. Davis (2001) found that $\alpha = 0.5 \pm 0.02$ for a heavily piled-up quasar. However, this grade migration parametrization is unlikely to perfectly describe the function. The parameter α may vary depending on the degree of pileup and the energy of the photons, therefore on the incident

⁷ For discussion of pileup analysis, see <http://space.mit.edu/CXC/analysis/davis/head2002/index.html>

⁸ see <http://space.mit.edu/CXC/analysis/PILECOMP/index.html> for discussion

spectrum, so we do not fix α . For low pileup spectra like X5 and X7, most of the pileup consists of only two photons. Thus only one parameter is needed to describe the grade migration for most of the pileup (effectively a normalization of the primary piled peak), and the exact form of the parametrization is not important. We confirm this by varying the parameter psfrac between 0.9 and 0.95 and letting other parameters vary. When psfrac is altered, α also varies in the opposite direction, but all other source parameters remain constant to roughly 1%. We find that the best fit value for α generally lies between 0.45 and 0.55 for all models that fit the spectrum accurately ($\chi^2_\nu < 1.2$).

Our interpretation of the pileup is supported by three small parts (4.6, 3.2, and 0.8 ksec) of the full *Chandra* dataset that we intentionally collected using a subarray mode to reduce the frame time to 0.9 s, and thus reduce pileup in any bright sources. ISIS fits suggest that the pileup fraction is 7 and 8% respectively for the full datasets of X5 and X7, but only 2% for the subarray exposures. The difference can be clearly seen between figure 3, the subarray exposure spectra of X5 (uneclipsed, 369 counts) and X7 (423 counts), compared to Figure 2 showing the full combined exposures of X5, excluding eclipses and dips (4181 counts), and X7 (5508 counts). The pileup bump beyond 2 keV is mostly removed in the subarray exposure.

REFERENCES

- Akmal, A., Pandharipande, V. R., & Ravenhall, D. G. 1998, *Phys. Rev. C* 58, 1804
- Arnaud, K. A. 1996, in G. Jacoby & J. Barnes, (eds.) *ASP Conf. Series Astronomical Data Analysis Software and Systems V.*, vol. 101, 17
- Asai, K., Dotani, T., Mitsuda, K., Hoshi, R., Vaughan, B., Tanaka, Y., & Inoue, H. 1996, *PASJ* 48, 257
- Barziv, O., Kaper, L., van Kerkwijk, M. H., Telting, J. H., & van Paradijs, J. 2001, *A&A* 377, 925
- Bejger, M., & Haensel, P. 2002, *A&A* (in press; astro-ph/0209151)
- Bildsten, L., Salpeter, E. E., & Wasserman, I. 1992, *ApJ* 384, 143
- Blandford, R. D. & Begelman, M. C. 1999, *MNRAS* 303, L1
- Brown, E. F., Bildsten, L., & Rutledge, R. E. 1998, *ApJ* 504, L95 (BBR98)
- Burderi, L., D'Antona, F., & Burgay, M. 2002, *ApJ* 574, 325
- Burwitz, V., Haberl, F., Neuhauser, R., Predehl, P., Trümper, J., & Zavlin, V. E. 2002, *A&A* (in press; astro-ph/0211536)
- Campana, S., et al. 2002, *ApJ* 575, L15
- Campana, S., Colpi, M., Mereghetti, S., Stella, L., & Tavani, M. 2001, *ApJ* 561, 924
- Campana, S. & Stella, L. 2000, *ApJ* 541, 849
- Campana, S., Colpi, M., Mereghetti, S., Stella, L., & Tavani, M. 1998a, *A&ARv* 8, 279
- Campana, S. et al., 1998b, *ApJ* 499, L65
- Campana, S., Mereghetti, S., Stella, L., & Colpi, M. 1997, *A&A* 324, 941
- Chandler, A. M. & Rutledge, R. E. 2000, *ApJ* 545, 1000
- Colpi, M., Geppert, U., Page, D., & Possenti, A. 2001, *ApJ* 548, L175
- Daltabuit, E., & Cox, D. P. 1972, *ApJ* 177, 855
- Daniel, W. W. 1990, *Applied Nonparametric Statistics, 2nd Ed.*, PWS-Kent
- Davis, J. E. 2001, *ApJ* 562, 575
- Deufel, B., Dullemond, C. P., & Spruit, H. C. 2001, *A&A* 377, 955
- Edmonds, P. D., Heinke, C. O., Grindlay, J. E., & Gilliland, R. L. 2002, *ApJ* 564, L17
- Eracleous, M., Halpern, J., & Patterson, J. 1991, *ApJ* 382, 290
- Frank, J., King, A., & Raine, D. 1992, *Accretion Power in Astrophysics, 2nd ed.*, Cambridge University Press
- Freire, P. et al. 2001, *ApJL* 557, L105
- Gänsicke, B. T., Braje, T. M., & Romani, R. W., 2002 *A&A* 386, 1001
- Gratton, R. G. et al. 1997, *ApJ* 491, 749
- Grindlay, J. E., Heinke, C. O., Edmonds, P. D., & Murray, S. S. 2001a, *Science* 292, 2290 (GHE01)
- Grindlay, J. E., Heinke, C. O., Edmonds, P. D., Murray, S. S., & Cool, A. M. 2001b, *ApJ* 563, L53
- Grindlay, J. E., Camilo, F., Heinke, C. O., Edmonds, P. D., Cohn, H. L., & Lugger, P. M., 2002 *ApJ* (in press; astro-ph/0208280)
- Houck, J. C. & DeNicola, L. A., 2000, *ASP Conf. Ser. Vol. 216: Astronomical Data Analysis Software and Systems IX*, eds. N. Manset, C. Veillet, and D. Crabtree, (Astronomical Society of the Pacific), 591
- Howell, J. H., Guhathakurta, P. & Gilliland, R. L., 2000, *PASP* 112, 1200
- Hurley, J. & Shara, M. 2002, *ApJ* 570, 184
- Illarionov, A. F. & Sunyaev, R. A. 1975, *A&A* 39, 185
- in't Zand, J. J. M., van Kerkwijk, M. H., Pooley, D., Verbunt, F., Wijnands, R., & Lewin, W. H. G. 2001, *ApJ* 563, L41
- Kallman, T. R., & McCray, R. 1982, *ApJS* 50, 263
- Kaminker, A. D., Haensel, P., & Yakovlev, D. G. 2001, *A&A* 373, L17
- Kong, A. K. H., McClintock, J. E., Garcia, M. R., Murray, S. S., & Barret, D. 2002, *ApJ* 570, 277
- Lattimer, J. M. & Prakash, M. 2001, *ApJ* 550, 426
- Lloyd, D. A., Hernquist, L., & Heyl, J. 2002, *ApJ* (submitted)
- Maccarone, T. J. & Coppi, P. S. 2002, *MNRAS* (in press; astro-ph/0209116)
- Menou, K., & McClintock, J. E. 2001, *ApJ* 557, 304
- Nath, N. R., Strohmayer, T. E., & Swank, J. H. 2002, *ApJ* 564, 353
- Nowak, M. A., Heinz, S., & Begelman, M. C. 2002, *ApJ* 573, 778
- Orosz, J. A. & Kuulkers, E. 1999, *MNRAS* 305, 132
- Parmar, A. N., White, N. E., Giommi, P., & Gottwald, M. 1986, *ApJ* 308, 199
- Predehl, P. & Schmitt, J. H. M. M. 1995, *A&A* 293, 889
- Protassov, R., van Dyk, D. A., Connors, A., Kashyap, F. L., Siemiginowska, A. 2002, *ApJ* 571, 545
- Rajagopal, M. & Romani, R. W. 1996, *ApJ* 461, 327
- Romani, R. 1987, *ApJ* 313, 718
- Rutledge, R. E., Bildsten, L., Brown, E. F., Pavlov, G. G., & Zavlin, V. E. 1999, *ApJ*, 514, 945
- Rutledge, R. E., Bildsten, L., Brown, E. F., Pavlov, G. G., & Zavlin, V. E. 2001a, *ApJ*, 551, 921
- Rutledge, R. E., Bildsten, L., Brown, E. F., Pavlov, G. G., & Zavlin, V. E. 2001b, *ApJ* 559, 1054
- Rutledge, R. E., Bildsten, L., Brown, E. F., Pavlov, G. G., & Zavlin, V. E. 2002a, *ApJ* 578, 405
- Rutledge, R. E., Bildsten, L., Brown, E. F., Pavlov, G. G., & Zavlin, V. E. 2002b, *ApJ* 577, 346
- Sanwal, D., Pavlov, G. G., Zavlin, Z. E., & Teter, M. A. 2002, *ApJ* 574, L61
- Scargle, J. D. 1982, *ApJ* 263, 835
- Stella, L., Priedhorsky, W., & White, N. E., 1987, *ApJ* 312, L17
- Thorsett, S. E., & Chakrabarty, D. 1999, *ApJ* 512, 288
- Timmes, F. X., Woosley, S. E., & Weaver, T. A. 1996, *ApJ* 457, 834
- van der Klis, M. 2000, *ARAA* 38, 717
- van Kerkwijk, M. H. 2001, in *ASP Conf. Ser. Proc. Jan van Paradijs Memorial Symposium*, ed. Van den Heuvel, Kaper, Rol
- van Paradijs, J., Verbunt, F., Shafer, R. A., Arnaud, K. A. 1987, *A&A* 182, 47
- van Straaten, S., Ford, E. C., van der Klis, M., Méndez, M., Kaaret, P. 2000 *ApJ*, 540, 1049
- Verbunt, F., Belloni, T., Johnston, H. M., van der Klis, M., Lewin, W. H. G. 1994, *A&A* 285, 903
- Verbunt, F. & Hasinger, G., 1998, *A&A* 336, 895
- Wijnands, R., Miller, J. M., Markwardt, C., Lewin, W. H. G., & van der Klis, M. 2001, *ApJ* 560, L159
- Wijnands, R., Guinazzi, M., van der Klis, M., Méndez, M. 2002, *ApJ* 573, L45
- Zampieri, L., Turolla, R., Zane, S., & Treves, A., 1995, *ApJ* 439, 849
- Zavlin, V. E., Pavlov, G. G. & Shibano, Yu. A. 1996, *A&A* 315, 141
- Zhang, S. N., Yu, W., & Zhang, W., 1998, *ApJ* 494, L71
- Zoccali, M., et al. 2001, *ApJ* 553, 733

TABLE A1
Spectral Model Parameters

| Model Parameter | X5 | X7 |
|--|----------------------|-----------------------|
| Blackbody, Z_{solar} absorption | | |
| kT, eV | 237^{+7}_{-1} | 217^{+5}_{-11} |
| $N_{H,22}^a$ | $.03^{+.02}_{-0}$ | $.03^{+.04}_{-0}$ |
| χ^2_{ν}/dof | 1.37/27 | 1.11/27 |
| Null hyp. prob. | 9.5% | 31% |
| PL flux % | 0^{+4}_{-0} | $0^{+0.6}_{-0}$ |
| R_{∞} , km | $1.86^{+.2}_{-.1}$ | $2.43^{+.5}_{-.1}$ |
| Lloyd H-atm, Z_{solar} | | |
| kT ^b , eV | 119^{+21}_{-18} | 84^{+13}_{-12} |
| $N_{H,22}^a$ | $0.09^{+.05}_{-.05}$ | $.13^{+.06}_{-.04}$ |
| χ^2_{ν}/dof | 1.38/26 | 1.20/26 |
| Null hyp. prob. | 10% | 22% |
| PL flux % | 0^{+3}_{-0} | $0^{+0.5}_{-0}$ |
| R ^b , km | $11.7^{+7.5}_{-3.5}$ | 34^{+22}_{-12} |
| M_{NS}^c | $1.4^{+0.7}_{-0.7}$ | 2.3 ± 0.1 |
| Gänsicke H-atm, Z_{solar} | | |
| kT ^b , eV | 140^{+17}_{-18} | 106^{+10}_{-1} |
| χ^2_{ν}/dof | 1.37/26 | 1.22/26 |
| R ^b , km | $8.2^{+4.0}_{-2.7}$ | $18.6^{+9.6}_{-5.1}$ |
| M_{NS}^c | $0.9^{+0.9}_{-0.9}$ | $2.1^{+0.4}_{-0.3}$ |
| Lloyd H-atm, $Z_{47 \text{ Tuc}}$, edge | | |
| kT ^b , eV | 101^{+21}_{-14} | 74^{+13}_{-8} |
| $N_{H,22}^a$ | $0.09^{+.08}_{-.05}$ | $0.11^{+.09}_{-.06}$ |
| χ^2_{ν}/dof | 1.25/24 | 0.73/24 |
| Null hyp. prob. | 18% | 83% |
| Edge E, eV | 660^{+45}_{-67} | 632^{+36}_{-52} |
| Max τ | $0.32^{+.31}_{-.20}$ | $0.56^{+.27}_{-.22}$ |
| PL flux % | $1.2^{+2.2}_{-1.2}$ | $0^{+0.5}_{-0}$ |
| R ^b , km | $19.0^{+8.8}_{-7.8}$ | 50^{+21}_{-15} |
| M_{NS}^c | $2.0^{+0.4}_{-0.6}$ | $2.7^{+0.2}_{-0.2}$ |
| Gänsicke H-atm, $Z_{47 \text{ Tuc}}$, edge | | |
| kT ^b , eV | 125^{+20}_{-16} | 94^{+11}_{-12} |
| χ^2_{ν}/dof | 1.26/24 | 0.74/24 |
| R ^b , km | $11.5^{+6.1}_{-4.0}$ | $27.2^{+10.6}_{-9.2}$ |
| M_{NS}^c | $2.0^{+0.4}_{-1.2}$ | $2.6^{+0.3}_{-0.4}$ |

Note. — All errors are 90% confidence limits. Distance of 4.50 kpc is assumed. Galactic column of 3×10^{20} is imposed as minimum N_H . ^a $N_{H,22}$ in units of 10^{22} cm^{-2} . ^b R, kT for assumed z of 0.306, implying 10 km, $1.4 M_{\odot}$ NS; this tests for consistency with the standard model. ^c Range of M_{NS} derived from allowed z values if radius fixed at 10 km.

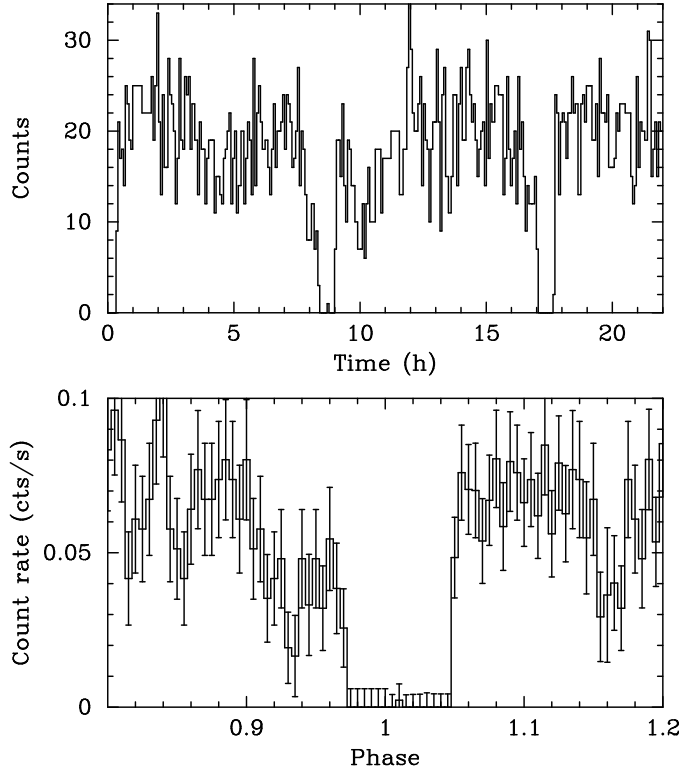


FIG. A1.— Top: Lightcurve of X5, showing the three eclipses and other dips. Bins are each 264 seconds long, and the small gaps between exposures have been removed. Bottom: Phase plot of the eclipse and pre-eclipse dip portion of X5's lightcurve, using 8.666 hour period. Bins are 156 s long.

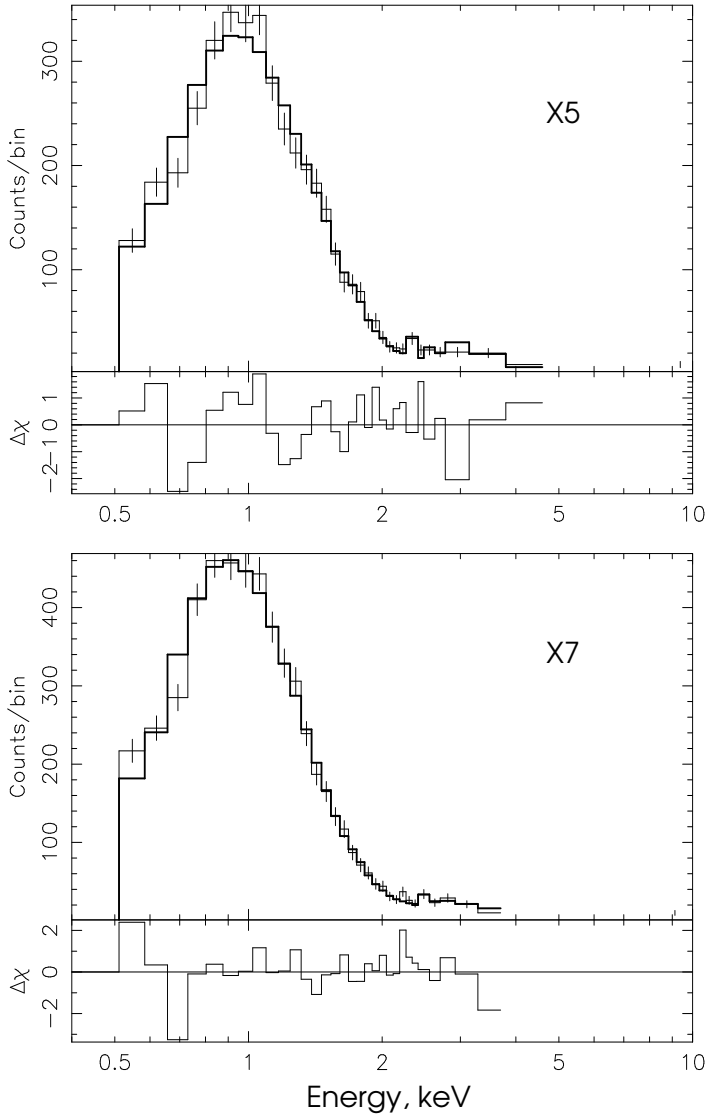


FIG. A2.— Data and best-fit Lloyd model spectra using hydrogen atmosphere model, solar metallicity gas for X5 and X7. Note the residual feature near 0.7 keV in both spectra, and lack of a harder component.

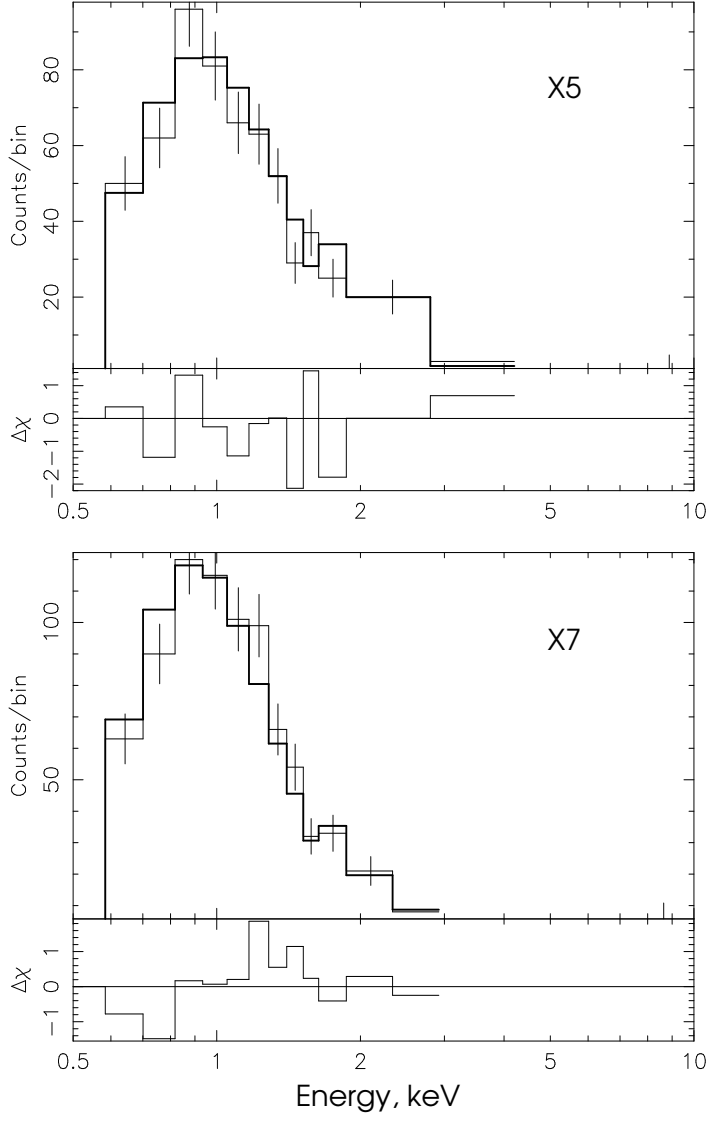


FIG. A3.— Best-fit Lloyd hydrogen atmosphere model to full datasets (as in Fig. 2), plotted over the subarray exposure data for X5 and X7. Note diminishment of pileup bump (compared to Fig. 2) beyond 2 keV due to smaller frame exposure times.

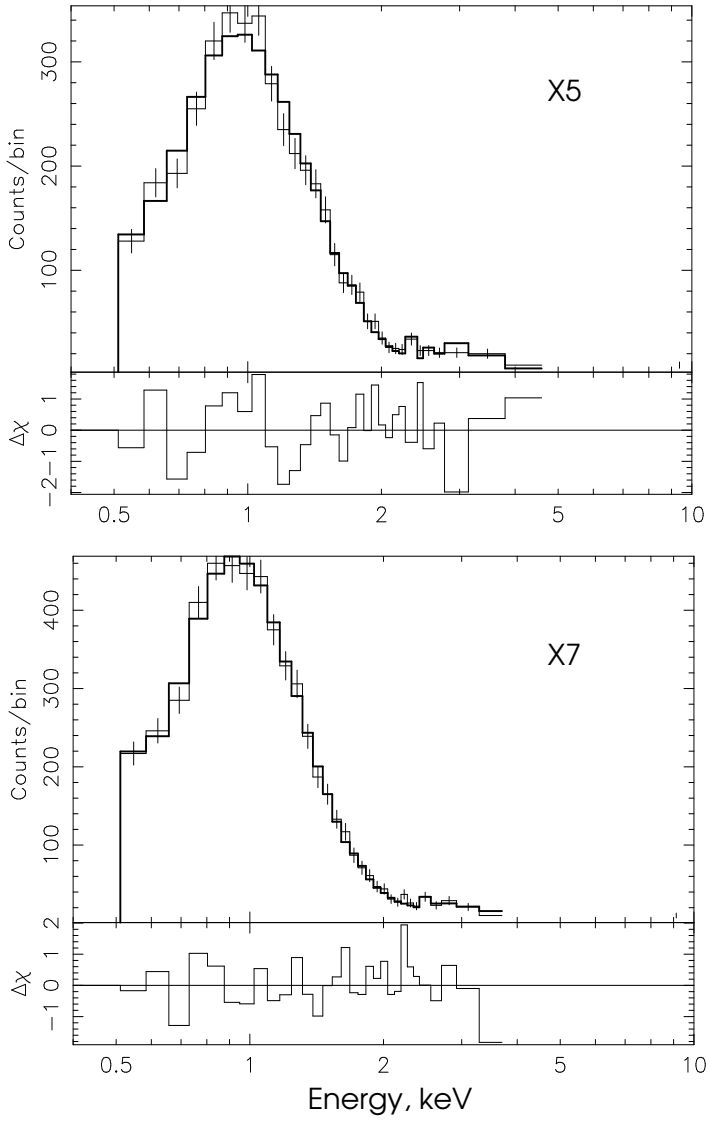


FIG. A4.— Data and best-fit model spectra for X5 and X7 using Lloyd hydrogen atmosphere model, 47 Tuc metallicity gas, and best-fitting edge. Note improvement in low-energy residuals for both X5 and X7 over Fig. 2.

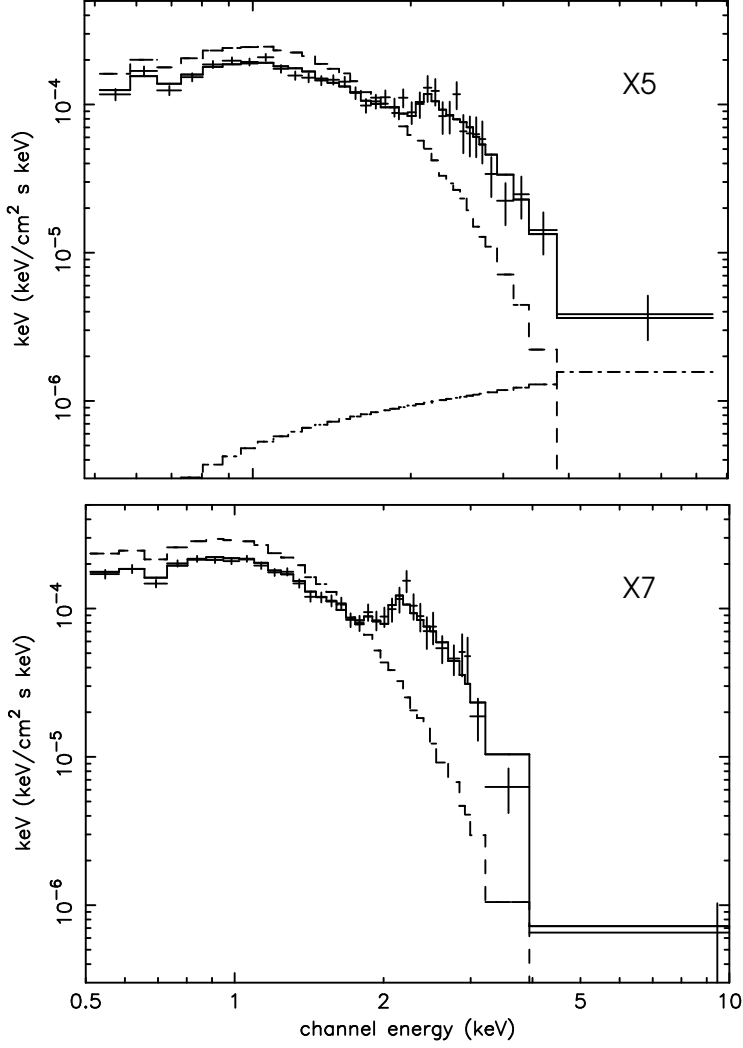


FIG. A5.— Data and model spectra (best-fit Lloyd hydrogen atmosphere with 47 Tuc metallicity gas, edge, PL), plotted in νF_ν space, of X5 and X7. The bump near 2 keV is an instrumental effect due to pileup, not unfolded but accounted for in the fit. The two components—the thermal hydrogen NS atmosphere, and the power law component—are displayed at their best-fit normalizations, which for X7 is not visible in this plot.

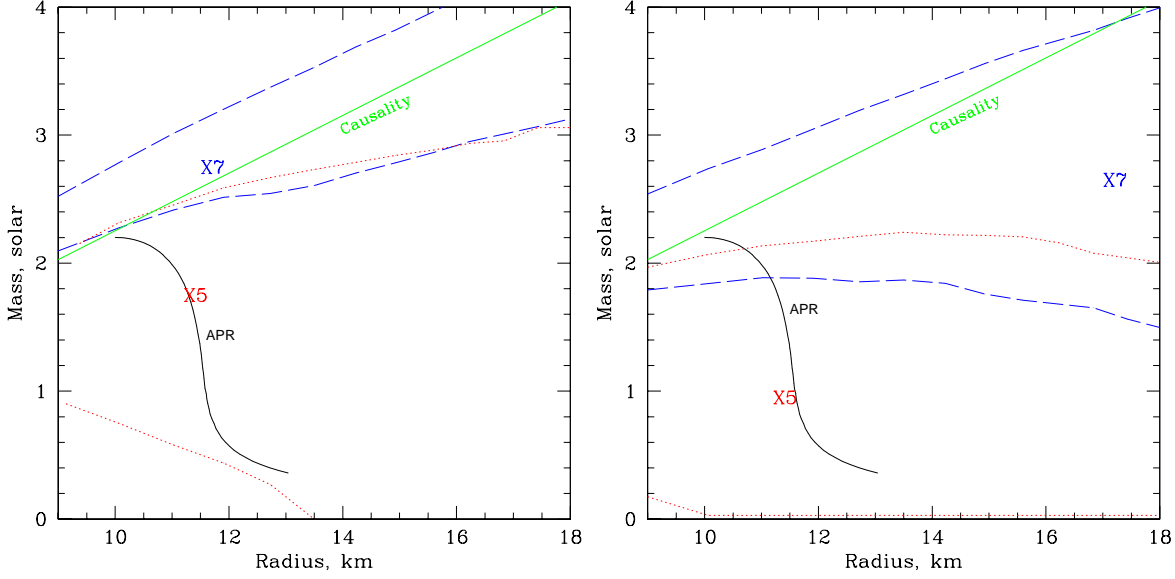


FIG. A6.— 90% confidence contours in the M-R plane for X7, (blue) long-dashed line, and X5, (red) dotted line, using the best-fit model with hydrogen atmosphere NS model, and standard photoelectric absorption. The left panel uses the Lloyd et al. (2002) hydrogen atmosphere model, while the right panel uses the Gänsicke et al. (2002) hydrogen atmosphere model. The labels “X5” and “X7” indicate the rough locations of the best fits. The causality constraint is plotted as the (green) solid line, and the APR model is plotted as the black curve. (See the electronic edition of *ApJ* for a color version of this figure.)

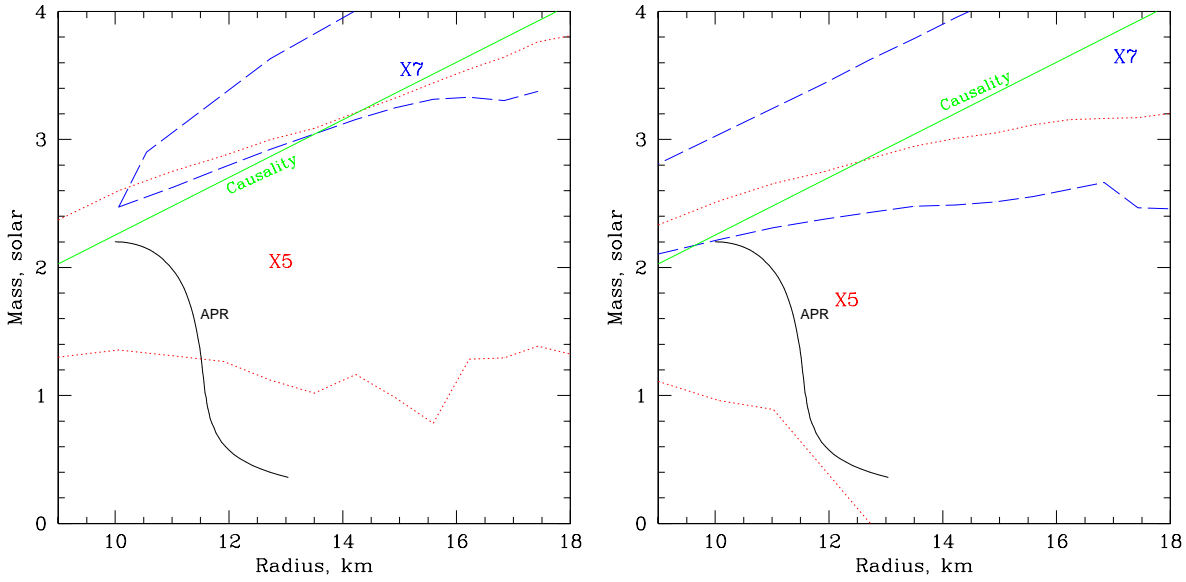


FIG. A7.— 90% confidence contours in the M-R plane for X7, (blue) long-dashed line, and X5, (red) dotted line, using the best-fit model with 47 Tuc metallicity absorbing gas, and a free edge. The left panel uses the Lloyd et al. (2002) hydrogen atmosphere model, while the right panel uses the Gänsicke et al. (2002) hydrogen atmosphere model. The labels “X5” and “X7” indicate the rough locations of the best fits. The causality constraint is plotted as the (green) solid line, and the APR model is plotted as the black curve. (See the electronic edition of *ApJ* for a color version of this figure.)